Earth and Planetary Science Letters 293 (2010) 368–376

Contents lists available at ScienceDirect

Earth and Planetary Science Letters

journal homepage: www.elsevier.com/locate/epsl

Biomineralization, crystallography and magnetic properties of bullet-shaped magnetite magnetosomes in giant rod magnetotactic bacteria

Jinhua Li [a], Yongxin Pan [a,b,*], Qingsong Liu [a,b], Kui Yu-Zhang [c], Nicolas Menguy [b,d], Renchao Che [e], Huafeng Qin [a], Wei Lin [a], Wenfang Wu [a], Nikolai Petersen [f], Xin'an Yang [g]

[a] Biogeomagnetism Group, Key Laboratory of the Earth's Deep Interior, Institute of Geology and Geophysics, Chinese Academy of Sciences, Beijing 100029, China
[b] France-China Bio-Mineralization and Nano-Structures Laboratory, Beijing 100029, China
[c] Laboratoire de Microscopies et d'Etude de Nanostructures (LMEN), Université de Reims, 59687 Reims, France
[d] Institut de Minéralogie et Physique des Milieux Condensés, UMR CNRS 7590, 75015 Paris, France
[e] Laboratory of Advanced Materials and Department of Material Science, Fudan University, Shanghai 200433, China
[f] Department of Earth and Environmental Science, Ludwig-Maximilians-Universität, D-80333 Munich, Germany
[g] Beijing National Laboratory for Condensed Matter Physics, Institute of Physics, Chinese Academy of Sciences, Beijing 100080, China

ARTICLE INFO

Article history:
Received 17 November 2009
Received in revised form 2 March 2010
Accepted 4 March 2010
Available online 29 March 2010

Editor: R.W. Carlson

Keywords:
magnetotactic bacteria
bullet-shaped magnetite magnetosome
biomineralization
crystallography
sedimentary magnetism

ABSTRACT

Magnetosomes produced by magnetotactic bacteria are of great interest for understanding bacterial biomineralization along with sedimentary magnetism and environmental magnetism. One of the most intriguing species, *Magnetobacterium bavaricum* can synthesize hundreds of bullet-shaped magnetite magnetosomes per cell, which contribute significantly to magnetic properties of sediments. However, the biomineralization mechanism and magnetic properties of such magnetosomes remain unknown. In this paper, we have conducted a comprehensive study of the crystallography and magnetic properties of bullet-shaped magnetosomes formed by uncultivated giant rod magnetotactic bacteria (referred to as MYR-1), recently discovered in Lake Miyun (Beijing, China). Transmission electron microscopy observations reveal that each MYR-1 cell contains hundreds of bullet-shaped magnetite magnetosomes, which are arranged into 3 - 5 braid-like bundles of chains. The formation of the bullet-shaped magnetosomes can be divided into two stages: initial isotropic growth (up to ~ 20 nm) followed by elongation along the [100] direction, which is unusual compared with the expected [111] magnetic easy axis. Although the [100] orientation is the hard axis of the face-centered cubic magnetite, the shape anisotropy of bullet-shaped magnetosomes and intra-bundle magnetostatic interactions confine the magnetization direction of the chain along the long axis of the cell/bundle. Due to each bundle of magnetosome chains effectively behaving as an elongated single domain particle, the MYR-1 cells show high coercivity, weak intra-bundle magnetostatic interaction, and high δ-ratio. These results provide new insights into the biomineralization process and magnetic properties of bullet-shaped magnetite magnetosomes.

1. Introduction

Magnetotactic bacteria (MTB) have the ability of synthesizing intracellular nanometer-sized magnetite (Fe_3O_4) and/or greigite (Fe_3S_4) magnetosomes, which are usually organized into chain structures (Bazylinski and Frankel, 2004; Faivre and Schüler, 2008; Komeili, 2007). Recently, magnetosomes have attracted much attention because (1) they serve as an ideal system to understand the biomineralization process and the magnetite-based magnetoreception (Frankel and Bazylinski, 2006; Komeili et al., 2006; Pan et al., 2004; Pradel et al., 2006; Scheffel et al., 2006); (2) fossil magnetosomes (also called magnetofossils) could be suitable biomarkers for searching early terrestrial or extraterrestrial life and as potential proxies for reconstructing paleoenvironment (Kopp and Kirschvink, 2008; Kopp et al., 2009; McKay et al., 1996; Schumann et al., 2008; Thomas-Keprta et al., 2002); and (3) functionalized magnetosomes have potential applications as novel magnetic nano-biomaterials in biomedical and biotechnological fields (Lang et al., 2007; Matsunaga et al., 2007).

The growth morphology and crystal structure of magnetosomes have been studied by various techniques, such as transmission electron microscopy (TEM) and selected area electron diffraction (SAED) (Isambert et al., 2007; Lins et al., 2005; Mann et al., 1984a; Mann et al., 1987a,b; Meldrum et al., 1993a,b; Pósfai et al., 2007; Sparks et al., 1990; Taylor et al., 2001). Generally, magnetotactic spirilla, including *Magnetospirillum magnetotacticum* MS-1, *Magnetospirillum gryphiswaldense* MSR-1, *Magnetospirillum magneticum* AMB-1 and marine spirillum MMS-1 (formerly known as MV-4), produce

* Corresponding author. Biogeomagnetism Group, Key Laboratory of the Earth's Deep Interior, Institute of Geology and Geophysics, Chinese Academy of Sciences, Beijing 100029, China. Tel.: +86 10 8299 8406.
E-mail address: yxpan@mail.iggcas.ac.cn (Y. Pan).

0012-821X/$ – see front matter © 2010 Elsevier B.V. All rights reserved.
doi:10.1016/j.epsl.2010.03.007

equiaxial or elongated cubo-octahedral magnetite magnetosomes (Mann et al., 1984a; Meldrum et al., 1993b; Pósfai et al., 2007). In contrast, magnetotactic vibrios and cocci, e.g., the marine vibrio strains MV-1 and MV-2 and the marine coccus MC-1 (Meldrum et al., 1993a,b), synthesize elongated prismatic magnetite magnetosomes. One common feature of these species is that the magnetosomes within the bacteria are always arranged into a single chain with both the crystal elongation and the chain parallel to the magnetocrystalline easy axis ([111]) of magnetite (Fe_3O_4). Furthermore, pulse magnetic-field measurements and electron holographic imaging on individual cells both confirm that the magnetosome chains behave as a single domain (SD) particle due to the joint contribution of the magnetocrystalline anisotropy and shape anisotropy of individual magnetosomes, and the intra-chain magnetostatic interactions (Dunin-Borkowski et al., 1998; Hanzlik et al., 2002; Pósfai et al., 2007; Penninga et al., 1995; Simpson et al., 2005). However, other elongation directions have also been reported for the highly anisotropic bullet-shaped magnetite magnetosomes, e.g., [100] (Isambert et al., 2007; Lins et al., 2007; Pósfai et al., 2006; Taylor et al., 2001; Vali and Kirschvink, 1990), [110] (Taylor and Barry, 2004), or [112] (Mann et al., 1987a,b). To further understand the biomineralization of these special magnetosomes, studies of the crystallography and magnetic properties of the bullet-shaped magnetosomes and of their effects on the cell's magnetotaxis are essential.

The *Magnetobacterium bavaricum* and similar types of bacteria have been found in Lake Chiemsee, Germany (Hanzlik et al., 1996; Pan et al., 2005b; Spring et al., 1993; Vali et al., 1987), at Koganei, Japan (Thornhill et al., 1994), in the Seine river, France (Isambert et al., 2007), and in Lake Miyun, China (Lin et al., 2009). These bacteria form hundreds up to a thousand of intracellular bullet-shaped magnetosomes, which are usually arranged into bundles of magnetosome chains (Isambert et al., 2007; Lin et al., 2009; Pan et al., 2005b; Spring et al., 1993; Thornhill et al., 1994). Phylogenetic analyses reveal that these MTBs are affiliated with the *Nitrospira* phylum, i.e., they belong to the same evolutionary lineage of MTB, possibly the oldest MTB (Lin et al., 2009; Spring et al., 1993). Recent studies have revealed that MTB affiliated with the *Nitrospira* phylum, but having cell morphology and size distinctly different from *M. bavaricum*, i.e., short vibrios and cocci, can also produce bullet-shaped magnetosomes and organize them into bundled chains (Flies et al., 2005; Lin et al., 2009). Bullet-shaped magnetite magnetosomes are also observed together with greigite magnetosomes within multicellular magnetotactic prokaryotes (MMP) which are affiliated to *Deltaproteobacteria* (Lins et al., 2007). Due to the wide distribution of *Nitrospira* and *Deltaproteobacteria* MTB, bullet-shaped magnetite magnetosomes may contribute significantly to iron cycling and sedimentary magnetism within a range of sedimentary environments (Pan et al., 2005a; Spring et al., 1993). However, the biomineralization process and magnetic properties of such bullet-shaped magnetite magnetosomes are still poorly understood, because (1) culturing these bacteria has been unsuccessful until now, and (2) the enrichment of cells in sufficient quantities is difficult.

In this study, we report the crystallographic habits and bulk magnetic properties of bullet-shaped magnetosomes produced within uncultivated giant rod MTB, recently isolated from Lake Miyun, hereafter designed as MYR-1. The aims of this study are (1) to investigate the biologically controlled mineralization process (via the growth of bullet-shaped magnetosomes), and (2) to understand the relationship between crystal orientations, spatial chain(s) arrangements and bulk magnetic properties of magnetosomes within MYR-1 cells.

2. Samples and methods

2.1. Sampling and enrichment of MYR-1 cells

Surface sediments from Lake Miyun were collected at water depth of 3-10 m with a long-handled scoop bucket. To setup microcosms in laboratory, samples were divided into 50 plastic bottles (~ 600 ml) and were stored in dimmed light at room temperature with a proportion of approximately 3:1 for sediment:water mix. Two microcosms were found to be dominated by rod MYR-1 (Fig. 1a). Living MYR-1 cells in the sediment were magnetically concentrated using a double-ended open magnetic separation apparatus ('MTB trap') (Jogler et al., 2009).

2.2. Transmission electron microscopy (TEM) study

The concentrated MYR-1 suspension was deposited onto carbon-coated copper grids or ultrathin carbon-coated holey grids for TEM observations. Intact cells were studied unstained or after staining with 1% uranyl acetate. For lattice imaging and electron diffraction, isolated magnetosomes were collected after NaOH solution digestion of the cells that were air-dried on the grids (1 M NaOH for 10 min at room temperature followed by washing with distilled water). All specimens were protected in nitrogen atmosphere and kept frozen to prevent possible oxidation prior to measurements. TEM observations were carried out on a JEM2010 microscope operating at 200 kV. SAED patterns were recorded on groups of magnetosomes as well as individual magnetosomes. The energy dispersive X-ray spectroscopy (EDXS) analyses were carried out on a JEM 2100F microscope equipped with an Oxford TEM200 EDXS. Digital Micrograph software was used for image processing (filtering of high resolution TEM (HRTEM) images and obtaining Fast Fourier transform (FFT) patterns). Magnetosome dimensions were measured from the TEM micrographs along their long axis (length) and maximum width perpendicular to the long axis (width).

2.3. Magnetic measurements

Two types (randomly oriented, and magnetically oriented) of bulk cell samples were chosen for magnetic measurements. To orient cells, a drop of the solution containing the living MYR-1 cells was placed onto a small piece of non-magnetic cover slide (~ 0.3×0.3 cm), and then the slide was placed between a pair of disk magnets during the solvent evaporation. To avoid possible oxidation, the cell sample preparation was undertaken within an anaerobic glove box.

Room-temperature magnetic experiments were performed using a Princeton AGM2900 test apparatus with a sensitivity of 1.0×10^{-11} Am^2. Hysteresis loops were measured between $\pm$ 1 T. Saturation magnetization (M_s), saturation remanence (M_{rs}) and coercivity (B_c) were determined after correction for linear contributions from the diamagnetic and paramagnetic phases. The saturation isothermal remanence magnetization (SIRM) was demagnetized in a backfield to determine the remanence coercivity (B_{cr}). First-order reversal curve (FORC) measurements were conducted following the protocol described by Roberts et al. (2000). A total of 130 FORCs were measured for each sample. FORC diagrams were calculated by using the FORCinel version 1.05 software with a smoothing factor of 3 (Harrison and Feinberg, 2008). In order to determine the effects of the chain configuration on magnetic properties, the oriented sample was measured at angles of 0°, 45° and 90° with respect to the long axis of the chain/cell.

Low-temperature magnetic experiments were performed using a Quantum Design Magnetic Property Measurement System (MPMS XP-5) with a sensitivity of 5.0×10^{-10} Am^2 and a residual field of less than 0.2 mT. Zero-field cooled (ZFC) and field cooled (FC) curves were acquired by cooling the sample in a zero field and in a 2.5 T field from 300 K to 5 K, respectively, giving the sample a saturation remanence in a 2.5 T field at 5 K (hereafter termed $SIRM_{5K\_2.5T}$) and measuring the remanence during warming from 5 K to 300 K in zero field. Thermal dependence of SIRM, obtained by saturating the sample in a 2.5 T field at 300 K (hereafter termed $SIRM_{300K\_2.5T}$), was measured in a zero field during a cooling-warming cycling (300→5→300 K).

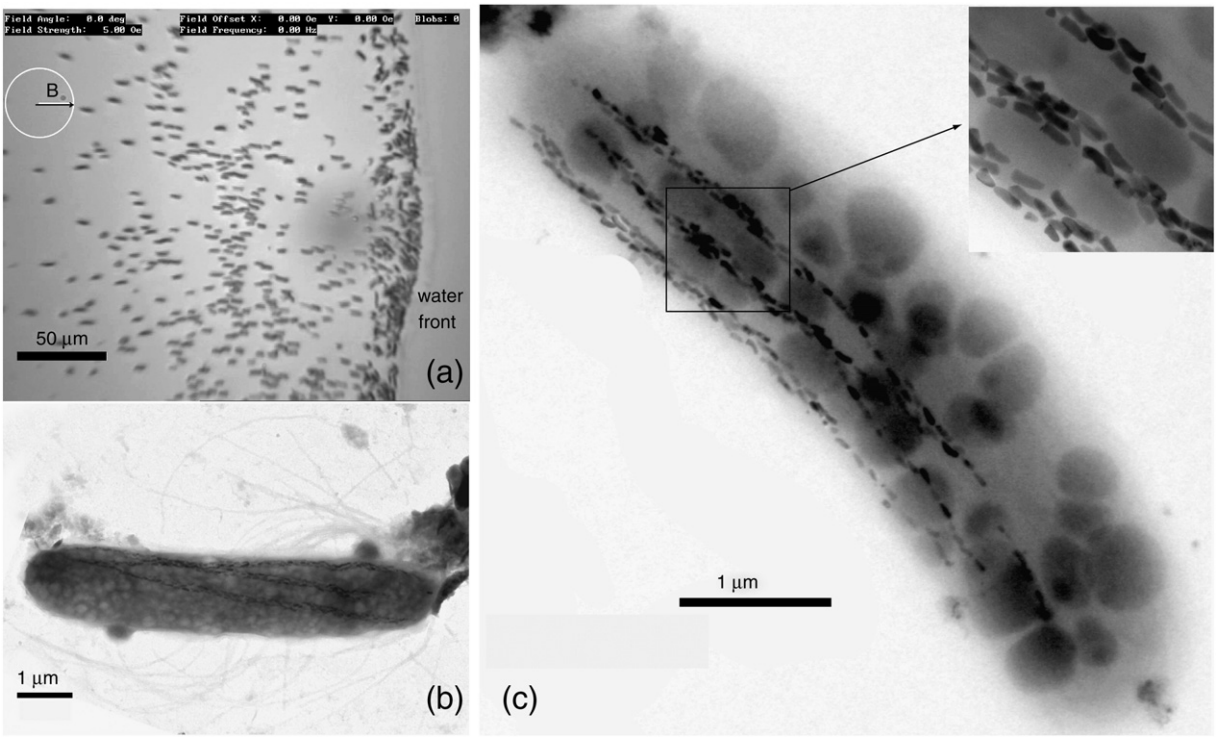

Fig. 1. (a) Optical micrograph of MYR-1 cells enriched with a Bacteriodrome system. Note that the applied field (B = 0.5 mT) direction points to the right, MYR-1 cells are swimming towards the water droplet edge. (b) One uranyl-acetate-stained MYR-1 cell showing single-polar-tufted flagella. (c) One unstained MYR-1 cell with an enlarged region showing intracellular bullet-shaped magnetosomes and their chains (bundles).

3. Results

3.1. Morphology of cells and chain arrangement of magnetosomes

Both light microscopy and electron microscopy observations show that the enriched cell samples contain solely giant rod MYR-1 cells (Fig. S1). The width of MYR-1 cells is relatively uniform (1.0 to 2.2 μm; average, 1.5 ± 0.3 μm), but the length varies significantly (4 to 13 μm; average, 6.5 ± 1.5 μm). Each cell has a single polar tuft of flagella (Fig. 1b), and contains hundreds of magnetosomes that are organized into 3 to 5 braid-like bundles of chains. Each bundle is comprised of two or three magnetosome chains shifted with respect to one another by less than a magnetosome length. Larger magnetosomes have a bullet shape with the long axis approximately parallel to the magnetosome chains, and smaller magnetosomes of spherical or elongated rectangular shapes are located at two ends of magnetosome chains (Fig. 1c). It is also noted that the tips of magnetosomes do not all point to the same direction. The majority of magnetosomes (> 85%) are found to be assembled in the same direction, with others in the opposite direction. In addition, cells of MYR-1 usually contain intracellular dark and white globules, which are identified respectively as sulfur-rich and lipid storage granules based on the EDXS analyses (Fig. S2). According to previous studies (Isambert et al., 2007; Lefèvre et al., 2009; Silva et al., 2008; Spring et al., 1993), the lipid and sulfur granules within MTB cells can serve as temporary storage compounds.

3.2. Biomineralization and crystallographic habits of magnetosomes

Study by SAED technique of both individual and a cluster of magnetosomes indicates that the MYR-1 magnetosomes are pure magnetite. The measured *d* spacings are 4.86, 4.15, 2.95 and 2.51 Å, errors less than 1%. These spacings correspond to the (111), (200), (220) and (311) planes of face-centered cubic (fcc) Fe_3O_4.

Investigations of the distributions of grain length, width and shape factor (width/length), as well as the plot of shape factor versus length of the MYR-1 magnetosomes (Fig. S3), indicate that both the length and width distribution are asymmetric with a negative skewness of - 0.60 and - 0.46, respectively (Figs. S3a, b). Magnetosome length varies over a wide range (10 - 180 nm) with a mean value of 104 ± 31 nm (Fig. S3a), whereas the range of width values is relatively narrow (10 - 56 nm) with a mean value of 38 ± 6 nm (Fig. S3b). The shape factor has a maximum frequency around 0.32, and its distribution is asymmetric with a cut-off toward the smaller values (Fig. S3c). The MYR-1 magnetosomes fall well within the SD region when plotted on a magnetic phase diagram (Butler and Banerjee, 1975; Muxworthy and Williams, 2009) (Fig. S3d). The plot of particle length versus width indicates that for smaller values of magnetosome width up to ~ 20 nm, the length/width ratio is roughly 1 and their relationship is linear, for particles larger than ~ 20 nm, the length/width ratio become progressive larger. This suggests that the magnetosomes initially grow in an equidimensional form up to a size of ~ 20 nm, after which the length increases at a greater rate than the width. When the magnetosomes reach a width of about 40 nm, the crystals grow in length only (Fig. 2).

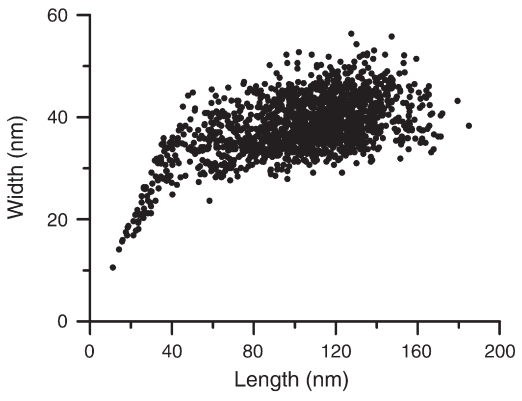

Fig. 2. Plot of length versus width of the MYR-1 magnetosomes.

This indicates a two-stage process of crystal growth for the MYR-1 magnetosomes.

The morphology and crystallography of the MYR-1 magnetosomes were determined by lattice imaging. Small magnetosomes (< 20 nm) are found to be isometric with ill-defined morphology (Fig. 3a, b), which presumes an isotropic growth of magnetosomes at their early stages. In contrast, large magnetosomes possess an elongated bullet shape indicating subsequent anisotropic growth. Based on lattice images viewed along the [001], [011], and [013] zone axes, the final elongation of crystals is determined to be always the [100] direction (Figs. 3c, d, and Fig. S4).

HRTEM analyses also indicate that the MYR-1 magnetosomes are well-crystallized. There is no evidence for the presence of detectable structural defects or non-crystalline regions within or overlying the

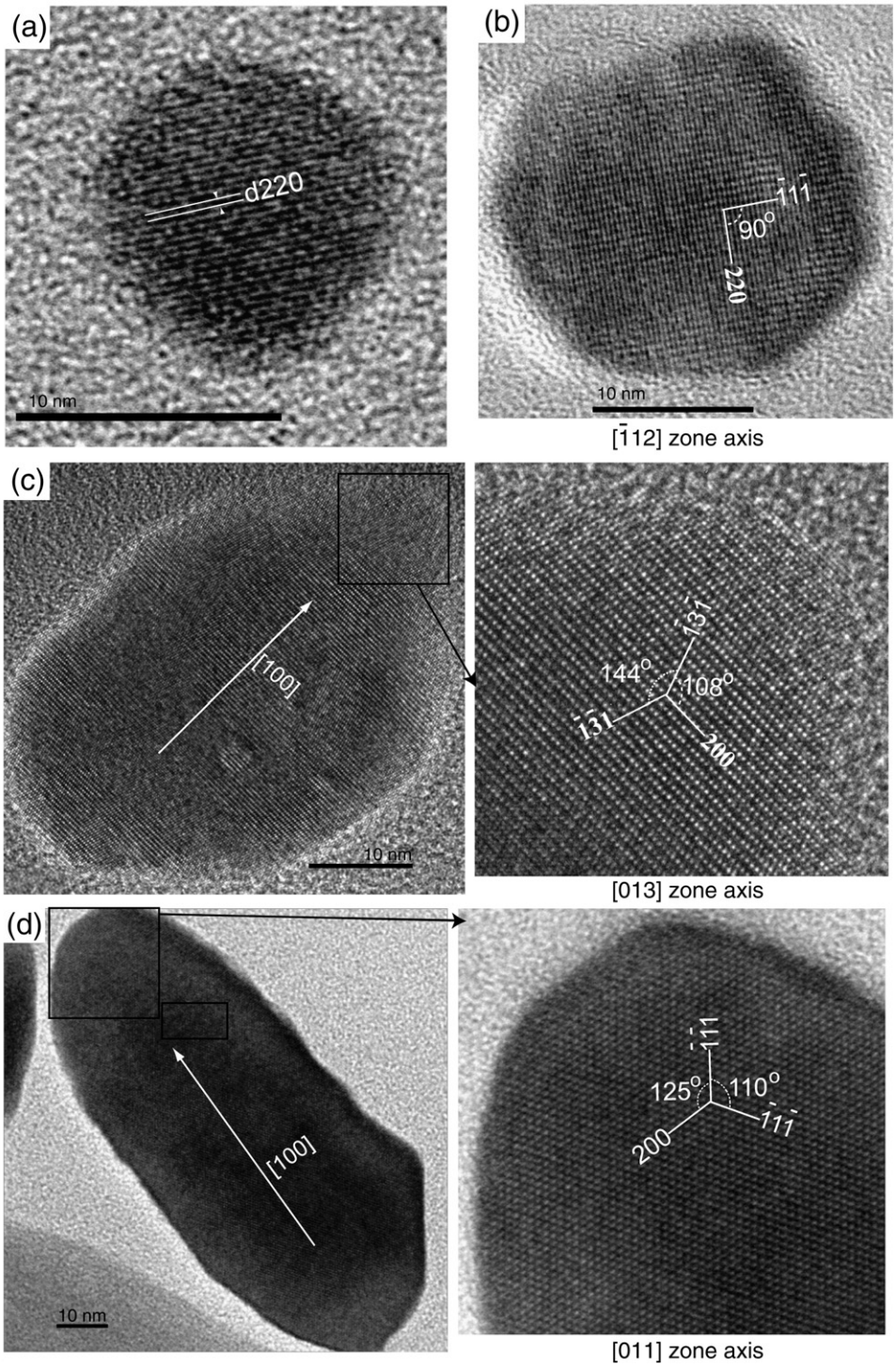

Fig. 3. HRTEM images showing a two-stage crystal growth process and crystal elongation along the [100] direction for the MYR-1 magnetosomes. (a) HRTEM image of a baby isometric magnetosome crystal (~ 10 nm), one set of (220) planes is running continuously across the particle. (b) [$\bar{1}$12] projection of a small magnetosome (~ 22 nm in diameter). Well-formed {111} and {110} planes coexist with ill-defined faces of the same index on the opposite side of the crystal. (c) [013] projection of an elongated magnetite particle with length and width of ~ 52 nm and ~ 36 nm, respectively. Lattice spacings corresponding to the (200), ($\bar{1}\bar{3}$1) and ($\bar{1}$3$\bar{1}$)planes, oriented at 108° and 144° to each other, respectively, are shown in the inset enlarged image. (d) [011] projection of a bullet-shaped magnetosome. Lattice spacings corresponding to the ($\bar{1}\bar{1}$1), ($\bar{1}$1$\bar{1}$) and (200) planes, oriented at 125° and 110° to each other, respectively, are shown in the inset enlarged image.

MYR-1 magnetosomes, i.e., twins or intergrowth boundaries. These features are commonly present within the magnetosomes produced by several cultivated MTB species or uncultivated *Bilophococcus magnetotacticus* (Devouard et al., 1998; Mann et al., 1984a,b; Meldrum et al., 1993a).

3.3. Room-temperature magnetic properties of MYR-1 cells

The hysteresis loop of the sample of randomly oriented MYR-1 cells has a pot-bellied shape (Fig. 4a) with hysteresis parameters B_c, B_{cr}, B_{cr}/B_c, M_{rs} and M_{rs}/M_s of 54.5 mT, 61.0 mT, 1.12, 1.25×10^{-8} Am^2 and 0.59, respectively, indicating characteristic uniaxial SD (USD) particle behavior (Dunlop and Özdemir, 1997).

The sample of oriented MYR-1 cells, as measured parallel to the cell long axes/magnetosome chain direction (0°), has a nearly square loop (Fig. 4b) with B_c, B_{cr}, B_{cr}/B_c, M_{rs} and M_{rs}/M_s values being 57.0 mT, 57.5 mT, 1.01, 2.25×10^{-8} Am^2 and 0.86, respectively. The hysteresis loop measured in a field inclined at 45° to the chain axis is pot-bellied (Fig. 4c), similar to that of the randomly oriented sample, with slightly larger values of B_c and M_{rs}/M_s but with a slighter lower B_{cr} value. When measured in a field perpendicular to the chains (90°), the hysteresis loop becomes significantly narrower and more slanting (Fig. 4d) than the other loops, with minimum values of B_c, M_{rs} and M_{rs}/M_s but a maximum of B_{cr}. Specifically, the hysteresis parameters B_c, B_{cr}, B_{cr}/B_c, M_{rs} and M_{rs}/M_s are 31.4 mT, 74.1 mT, 2.36, 0.38×10^{-8} Am^2 and 0.23, respectively. This indicates that the easy axis of magnetization of magnetosome chains is along the chain direction but the hard axis is perpendicular to it.

The domain state, magnetostatic interaction and the coercivity distribution of the magnetosomes within MYR-1 cells were further studied using FORC diagrams (Fig. 5). Overall, both the randomly oriented sample and the oriented sample exhibit typical SD behavior (Roberts et al., 2000). For the unoriented sample, the peak coercivity, $H_{c,FORC}$, which is defined as the H_c field corresponding to the peak of the FORC distribution, is 60.3 mT (Fig. 5a). For the oriented sample measured in a field inclined at 0°, 45° and 90° to the chain axis, the $H_{c,FORC}$ is 56.1 mT, 60.3 mT and 68.8 mT, respectively (Figs. 5b-d). It is also noted that the FORC diagram measured perpendicular to the chain axis is noisier than the others (Fig. 5d), possibly due to enhanced hardness of magnetization. However, the characteristic interaction field, $H_{b1/2}$, which is defined as the H_b field where the peak of the FORC distribution is reduced to half of its maximum value, is small (3.4 - 3.9 mT) for all measurements. The observed $H_{b1/2}$ values of MYR-1 are slightly larger than that of single-chain MTB cells, e.g., AMB-1 cells (~ 2.4 mT) (Li et al., 2010), but smaller than that of magnetosome-clustered MTB cells, e.g., *Magnetococcus yuandaducia* (~ 5.3 mT) (Lin and Pan, 2009). This suggests weak inter-bundle and inter-cell interactions within the MYR-1 cells.

3.4. Low-temperature magnetic properties of MYR-1 cells

As shown in Fig. 6a, the remanence kink on FC and ZFC warming curves around ~ 100 K indicates the Verwey transition temperature (T_v) of magnetosome magnetite. The δ_{FC} and δ_{ZFC}, which are used to estimate the magnitude of remanence lost through the Verwey transition of the FC-SIRM$_{5K_2.5T}$ and ZFC-SIRM$_{5K_2.5T}$ warming curves, are 0.12 and 0.038, respectively, lower than for other types of MTB cells or isolated magnetosome samples (Li et al., 2009, 2010; Lin and Pan, 2009; Moskowitz et al., 1993; Pan et al., 2005b). This is possibly due to the [100] orientation of individual magnetosomes along the chains and/or strong positive intra-chain/bundle interaction. However, the FC-ZFC curves bifurcate below T_v with the FC remanence much greater than the ZFC remanence, and the δ-ratio is 3.1, higher than the threshold of the Moskowitz test value of 2.0 (Moskowitz

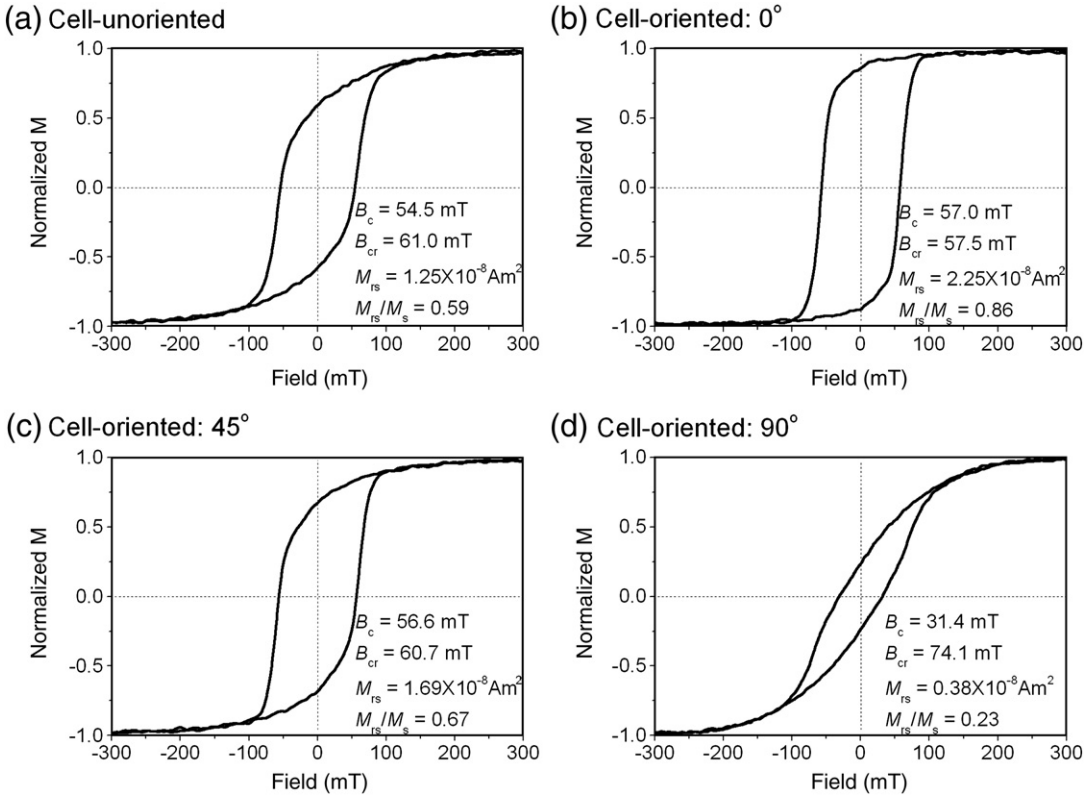

Fig. 4. Normalized hysteresis loops for: (a) the randomly oriented MYR-1 sample, (b, c and d) the magnetically oriented MYR-1 sample measured at 0°, 45° and 90° with respect to the long axis of cells. Net magnetization was obtained by subtracting background (blank glass cover slide).

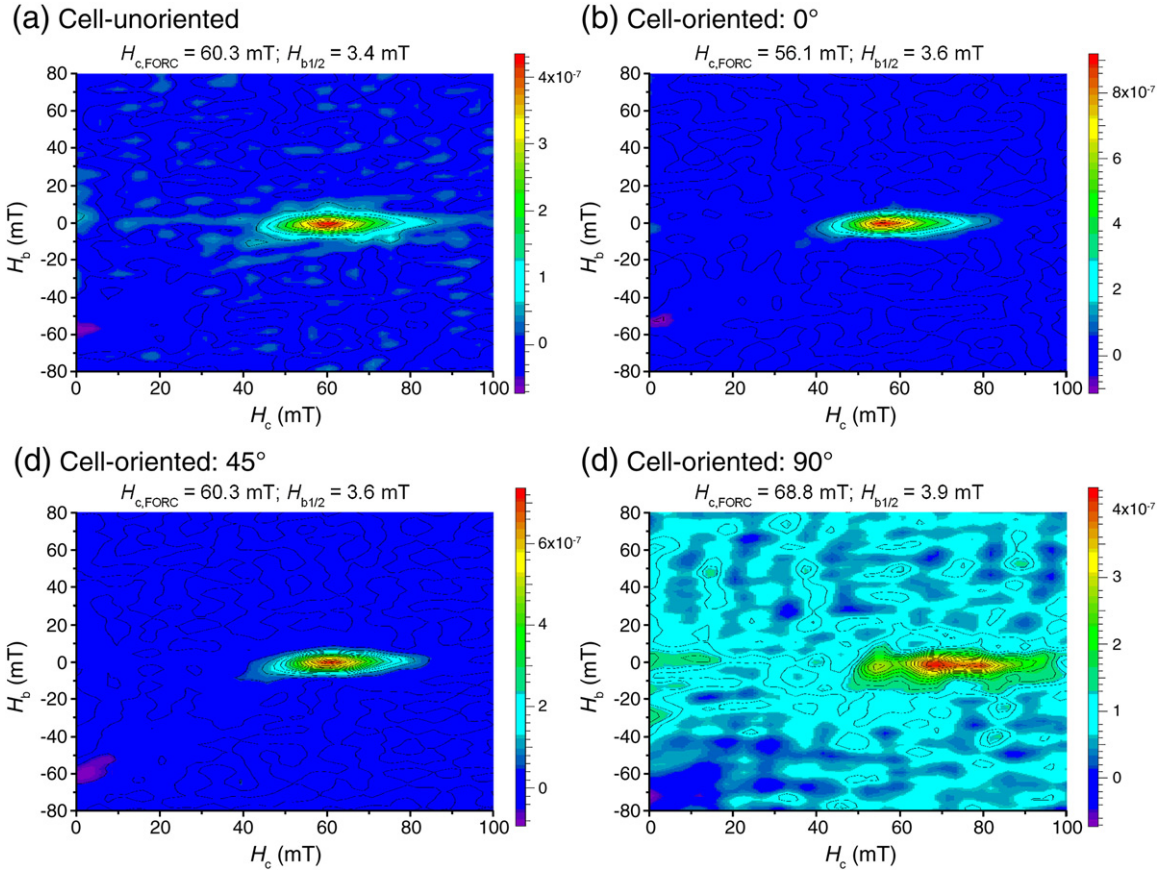

Fig. 5. FORC diagrams for: (a) the randomly oriented sample, (b, c and d) the magnetically oriented sample measured at 0°, 45° and 90° with respect to the long axis of cells. The peak coercivity, $H_{c,FORC}$, is defined as the H_c field corresponding to the peak of the FORC distribution, and the characteristic magnetostatic interaction field, $H_{b1/2,}$ is defined as the H_b field where the peak of the FORC distribution is reduced to half of its maximum value. All FORC diagrams are calculated with a smoothing factor of 3.

et al., 1993). In addition, the sharp decrease of remanence below 30 K can be related to the strong dipolar inter-particle interaction within magnetosome bundles (Prozorov et al., 2007), or to the superparamagnetic contribution of growing magnetosomes just below the threshold of SD/SP, or to the superficial maghematization of magnetosome magnetite (Moskowitz et al., 1993). The cooling-warming cycling curve of $SIRM_{300K\_2.5T}$ shows nearly reversible features (Fig. 6b). Upon cooling, the remanence gradually increases by about 7% down to ~ 100 K, and then reaches a plateau at lower temperatures. No distinct signal of the Verwey transition is observed (Fig. 6b).

4. Discussion

As mentioned above, magnetite magnetosomes for most MTB species are elongated and aligned along the [111] direction (Pósfai et al., 2007). This feature facilitates the mutual reinforcement of the effects of shape anisotropy and magnetocrystalline anisotropy of individual magnetosomes and inter-particle interaction within chains at room temperature, maximizing the total magnetic moment of magnetosomes, which makes it approximately equal to the sum of the individual magnetosome magnetic moments (Dunin-Borkowski et al., 1998; Simpson et al., 2005). In contrast, in MYR-1, the bacteria undergo a two-stage growth process, the first isotropic, the second involving elongation along the [100] crystallographic axis of magnetite. This unusual crystallographic habit means that the [111] easy magnetization axis is no longer parallel to the magnetosome chain axis, resulting in its magnetocrystalline anisotropy being different from the chain direction.

This [100] elongation has a pronounced effect on the low temperature properties of the magnetosomes. Generally, by cooling across the Verwey transition, magnetite undergoes a phase transition from its cubic phase above T_v to a monoclinic phase below it. Consequently, the easy magnetization axis of magnetite switches from $[111]_{cubic}$ to $[100]_{mono}$, and one of $<100>_{cubic}$ becomes the new monoclinic *c*-axis (also an easy magnetization axis) (Muxworthy and McClelland, 2000). This rotation of the easy magnetization axis is presumed to be responsible for the abrupt remanence changes at T_v. For magnetosome chains, the pronounced shape anisotropy of the chain structure causes the cubic *a*-axis nearest to the chain direction to preferentially become the monoclinic *c*-axis. When a strong magnetic field is applied during the cooling process, it can induce a partial alignment of this new magnetic easy axis in the direction of the cooling field, producing higher SIRM intensity below T_v. For the magnetosome chains with [111] orientations, e.g., AMB-1 magnetosomes (Li et al., 2010), the switching of easy magnetization axis between [111] and [100] at T_v inevitably results in some changes of magnetic signals. Actually, the magnetization direction of individual magnetosomes below T_v preferentially takes an equilibrium position between [111] and [100] due to the fact that the shape anisotropy of the chain and intra-chain interactions along the chain direction compete with the magnetocrystalline anisotropy (Moskowitz et al., 1993; Simpson et al., 2005), resulting in a lower δ value for magnetosome chain(s) compared with clustered magnetosome samples and chemically synthesized magnetite samples with the same grain-size range (Kopp et al., 2006; Li et al., 2010; Moskowitz et al., 1993; Pan et al., 2005b). For MYR-1 cells, both the original magnetization axes above T_v and the new monoclinic *c*-axes below T_v are the same along the [100] direction, thus the Verwey transition is

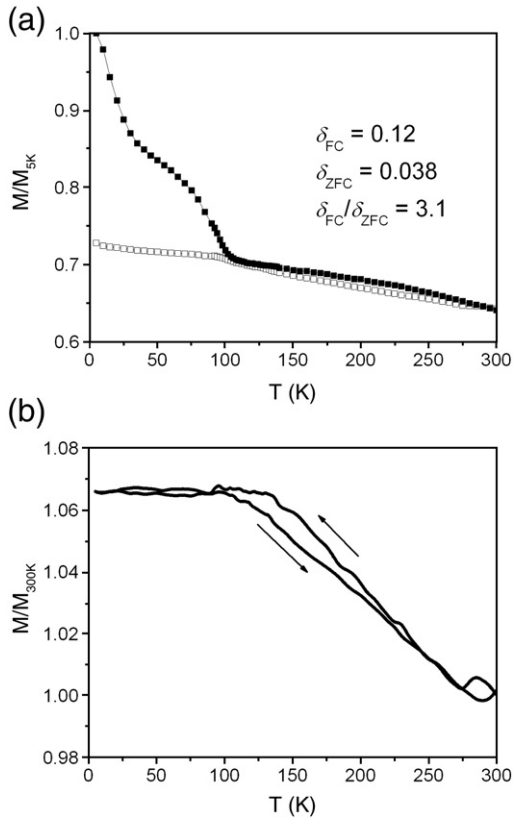

Fig. 6. Low-temperature magnetic properties of a sample of randomly oriented MYR-1 cells. (a) FC-SIRM$_{5K_2.5T}$ normalized FC-SIRM$_{5K_2.5T}$ (filled squares) and ZFC-SIRM$_{5K_2.5T}$ (open squares) warming curves. (b) Normalized SIRM$_{300K_2.5T}$ cooling-warming cycling curves.

highly smeared on the ZFC curves ($\delta_{ZFC}=0.038$) and even absent on the SIRM$_{300K_2.5T}$ cycling curve. However, strong field cooling through T_v would induce a partial alignment of one of the [100] directions closest to the field direction and enhance the initial SIRM$_{5K_2.5T}$ intensity, resulting in an enhanced Verwey transition on the FC curve ($\delta_{FC}=0.12$) and a high δ-ratio (3.1).

Based on theoretical modeling, Hanzlik et al. (2002) previously presumed that the polarity in magnetosome bundles within *M. bavaricum* was uniform and all bundles were magnetized parallel to the chain direction. In this study, the hysteresis loops and FORC diagrams of the orientated cell sample show a strong angular-dependence (Figs. 4 and 5). The significant difference of hysteresis parameters measured at different angles relative to the magnetosome chains indicates that the MYR-1 cell has pronounced magnetic anisotropy. Parallel to the magnetosome chain direction, the B_c and M_{rs} reach maximum, B_{cr} becomes minimum, whereas perpendicular to the magnetosome chain direction, the B_c and M_{rs} reach minimum, B_{cr} become maximum. These results indicate that despite of the elongation along the [100] axis rather than the [111] magnetocrystalline easy axis, each bundle of chains essentially acts as a single elongated SD particle with the easy axis aligned along the chain axis. This is consistent with previous observations and modeling of *M. bavaricum* (Hanzlik et al., 2002).

The magnetization of magnetosomes within MYR-1 parallel to the chain axis rather than along the [111] magnetocrystalline easy axis of individual crystals can be rationalized as compromise effects of shape anisotropy and intra-chain and intra-bundle interactions. That is to say, both the interactions within chains and the shape anisotropy of magnetosomes are parallel to the chain direction and therefore mutually reinforce to constrain the magnetization direction of individual particles uniformly along the chain direction. This is consistent with electron holography observations that show that the shape anisotropy of individual magnetosomes and the inter-particle interactions within chains appear to be the most important factors controlling their magnetization direction, whereas the magnetocrystalline anisotropy is less important (Dunin-Borkowski et al., 1998; Pósfai et al., 2007; Simpson et al., 2005). Our TEM observations reveal that two or three magnetosome chains are tightly assembled into one bundle with each chain shifted relative to each other in the axial direction by less than a magnetosome length. This configuration is energetically more favorable and stabilizes the bundles of magnetosomes allowing each individual magnetosomes to have uniform magnetization (Hanzlik et al., 2002). Therefore, the intra-chain and intra-bundle interactions may mutually reinforce each other's effects along the chain direction to completely overcome the effect of magnetocrystalline anisotropy. As a result, each bundle of magnetosome chains can behave as a large elongated SD particle. The magnetosome bundles are weakly interacting with each other due to the high shape anisotropy energy within bundles and large inter-bundle distances, which is confirmed by the FORC diagrams (Fig. 5).

Recent phylogenetic assignment and fluorescence *in-situ* hybridization (FISH) demonstrated that the MYR-1 is affiliated with *Nitrospira* phylum and shares a high degree of similarity of 16 S rRNA gene sequence with *M. bavaricum* (97.8%) (Lin et al., 2009). The present study reveals that the general features of MYR-1 are very similar to *M. bavaricum*, such as giant rod shape, comparable cell size, single-polar tufted flagella, numerous intracellular sulfur granules, bullet-shaped magnetite magnetosomes with 3 - 5 bundles of chains. Dimensional analysis and crystallographic studies unambiguously indicate that the MYR-1 magnetosomes have a two-stage crystal growth mechanism (Figs. 2 and 3). The earlier stage involves the development of isometric magnetite crystals, which grow up to ~ 20 nm. The later stage involves anisotropic growth elongated along the [100] direction. This sequence clearly differs from the two-stage growth process observed in ovoid MTB by Mann et al. (1987a,b), which starts from an isotropic cubo-octahedral morphology followed by anisotropic growth along the [112] direction. MYR-1 and *M. bavaricum* are closely related. The unusual magnetosome growth pattern in MYR-1 suggests that the *M. bavaricum* and similar types of bacteria may have a novel biomineralization pattern. However, the biomineralization mechanism is still unclear due to the lack of more detailed molecular studies on MYR-1 or *M. bavaricum*.

The magnetically easy, intermediate, and hard directions of magnetite are the <111>, <110>, and <100>, respectively, hence the crystal elongation along the [100] direction is energetically unfavorable and needs strictly biological control (Kirschvink, 1990; Mann et al., 1987a,b). Therefore, the bullet-shaped magnetite crystals in sediments, like those formed by MYR-1, unambiguously indicate their biogenic origins. That is to say, the bullet-shaped magnetite crystals could be used as a reliable biomarker in searching early terrestrial and extraterrestrial life or as a potential proxy for reconstructing paleoenvironment (Kopp et al., 2007; Mann et al., 1987a,b; Schumann et al., 2008). More crystallographic, magnetic and molecular studies of different MTB strains producing bullet-shaped magnetite magnetosomes are still essential to ultimately reveal their crystallographic habits, magnetic properties and biomineralization mechanism. Such studies would facilitate a better understanding of the paleomagnetic and paleoenvironmental implications of such bullet-shaped magnetofossils in the geological record.

5. Conclusion

The freshwater '*M. bavaricum*' - like MTB, MYR-1, has rod-shaped cell morphology with an average length of 6.5 μm and width of 1.5 μm, and possesses single-pole tufted flagella. It forms hundreds of bullet-shaped magnetosomes that are organized into 3 - 5 well-separated, braid-like bundles of magnetosome chains along the long axis of the cell. The magnetosomes have a wide range of crystal lengths from 10

to 180 nm (mean length 104 nm) and a relatively narrow range of crystal widths from 10 to 58 nm (mean width 38 nm).

Magnetosome morphologies studied by TEM/HRTEM provide lines of evidence for a two-stage crystal growth process involving an initially isotropic growth phase followed by anisotropic growth elongated along [100] and not along [111], as would be expected for fcc magnetite. This indicates that the magnetite magnetosomes in *M. bavaricum*-type MTB formed by a biomineralization mechanism that differs from that in other MTB that produce magnetosomes with [111] elongation.

Despite the [100] elongation and orientation, the pronounced shape anisotropy of individual magnetosomes and strong intra-bundle magnetostatic interaction may jointly contribute to the confinement of individual magnetic moments approximately parallel to the chain axis. In addition, the inter-cell and inter-bundle interactions are weak due to the fact that each bundle of magnetosome chains behaves as a large elongated SD particle and is well separated from the other bundles within the cell. The bullet-shaped magnetosomes produced by the giant rod MYR-1 may significantly increase the magnetic remanence of MTB or magnetofossil bearing sediments.

Acknowledgements

We thank L. Sun for the assistance with TEM observations, M. Pósfai for commenting on an earlier version of the manuscript, and G. A. Paterson for improving the English. We also thank R. W. Carlson and two anonymous reviewers for their very constructive comments. This work was supported by NSFC grants (40821091) and the CAS/SAFEA International Partnership Program for Creative Research Teams. Y. X. Pan and Q. S. Liu also thank supports from the '100 Talents Program' of CAS.

Appendix A. Supplementary data

Supplementary data associated with this article can be found, in the online version, at doi:10.1016/j.epsl.2010.03.007.

References

Bazylinski, D.A., Frankel, R.B., 2004. Magnetosome formation in prokaryotes. Nat. Rev. Microbiol. 2, 217–230.

Butler, R.F., Banerjee, S.K., 1975. Theoretical single-domain grain size range in magnetite and titanomagnetite. J. Geophys. Res. 80, 4049–4058.

Devouard, B., Pósfai, M., Hua, X., Bazylinski, D.A., Frankel, R.B., Buseck, P.R., 1998. Magnetite from magnetotactic bacteria: size distributions and twinning. Am. Mineral. 83, 1387–1398.

Dunin-Borkowski, R.E., McCartney, M.R., Frankel, R.B., Bazylinski, D.A., Pósfai, M., Buseck, P.R., 1998. Magnetic microstructure of magnetotactic bacteria by electron holography. Science 282, 1868–1870.

Dunlop, D.J., Özdemir, Ö., 1997. Rock magnetism: Fundamentals and Frontiers. Cambridge University Press, London. 1997.

Faivre, D., Schüler, D., 2008. Magnetotactic bacteria and magnetosomes. Chem. Rev. 108, 4875–4898.

Flies, C.B., Peplies, J., Schüler, D., 2005. Combined approach for characterization of uncultivated magnetotactic bacteria from various aquatic environments. Appl. Environ. Microbiol. 71, 2723–2731.

Frankel, R.B., Bazylinski, D.A., 2006. How magnetotactic bacteria make magnetosomes queue up. Trends Microbiol. 14, 329–331.

Hanzlik, M., Winklhofer, M., Petersen, N., 1996. Spatial arrangement of chains of magnetosomes in magnetotactic bacteria. Earth Planet. Sci. Lett. 145, 125–134.

Hanzlik, M., Winklhofer, M., Petersen, N., 2002. Pulsed-field-remanence measurements on individual magnetotactic bacteria. J. Magn. Magn. Mater. 248, 258–267.

Harrison, R.J., Feinberg, J.M., 2008. FORCinel: an improved algorithm for calculating first-order reversal curve distributions using locally weighted regression smoothing. Geochem. Geophys. Geosyst. 9. doi:10.1029/2008GC001987.

Isambert, A., Menguy, N., Larquet, E., Guyot, F., Valet, J.P., 2007. Transmission electron microscopy study of magnetites in a freshwater population of magnetotactic bacteria. Am. Mineral. 92, 621–630.

Jogler, C., Lin, W., Meyerdierks, A., Kube, M., Katzmann, E., Flies, C., Pan, Y.X., Amann, R., Reinhardt, R., Schüler, D., 2009. Toward cloning of the magnetotactic metagenome: Identification of magnetosome island gene clusters in uncultivated magnetotactic bacteria from Different Aquatic Sediments. Appl. Environ. Microbiol. 75, 3972–3979.

Kirschvink, J.L., 1990. On the magnetostatic control of crystal orientation and iron accumulation in magnetosome. Automedica 14, 257–269.

Komeili, A., 2007. Molecular mechanisms of magnetosome formation. Annu. Rev. Biochem. 76, 351–366.

Komeili, A., Li, Z., Newman, D.K., Jensen, G.J., 2006. Magnetosomes are cell membrane invaginations organized by the actin-like protein MamK. Science 311, 242–245.

Kopp, R.E., Kirschvink, J.L., 2008. The identification and biogeochemical interpretation of fossil magnetotactic bacteria. Earth-Sci. Rev. 86, 42–61.

Kopp, R.E., Raub, T.D., Schumann, D., Vali, H., Smirnov, A.V., Kirschvink, J.L., 2007. Magnetofossil spike during the Paleocene-Eocene thermal maximum: Ferromagnetic resonance, rock magnetic, and electron microscopy evidence from Ancora, New Jersey, United States. Paleoceanography 22. doi:10.1029/2007PA001473.

Kopp, R.E., Schumann, D., Raub, T.D., Powars, D.S., Godfrey, L.V., Swanson-Hysell, N.L., Maloof, A.C., Vali, H., 2009. An Appalachian Amazon? Magnetofossil evidence for the development of a tropical river-like system in the mid-Atlantic United States during the Paleocene-Eocene thermal maximum. Paleoceanography 24. doi:10.1029/2009PA001783.

Kopp, R.E., Weiss, B.P., Maloof, A.C., Vali, H., Nash, C.Z., Kirschvink, J.L., 2006. Chains, clumps, and strings: Magnetofossil taphonomy with ferromagnetic resonance spectroscopy. Earth Planet. Sci. Lett. 247, 10–25.

Lang, C., Schüler, D., Faivre, D., 2007. Synthesis of magnetite nanoparticles for bio- and nanotechnology: Genetic engineering and biomimetics of bacterial magnetosomes. Macromol. Biosci. 7, 144–151.

Lefèvre, C.T., Bernadac, A., Yu-Zhang, K., Pradel, N., Wu, L.F., 2009. Isolation and characterization of a magnetotactic bacterial culture from the Mediterranean Sea. Environ. Microbiol. 11, 1646–1657.

Li, J.H., Pan, Y.X., Chen, G.J., Liu, Q.S., Tian, L.X., Lin, W., 2009. Magnetite magnetosome and fragmental chain formation of *Magnetospirillum magneticum* AMB-1: Transmission electron microscopy and magnetic observations. Geophys. J. Int. 177, 33–42.

Li, J.H., Pan, Y.X., Liu, Q.S., Qin, H.F., Deng, C.L., Che, R.C., Yang, X.A., 2010. A comparative study of magnetic properties between whole cells and isolated magnetosomes of *Magnetospirillum Magneticum* AMB-1. Chin. Sci. Bull. 55, 38–44.

Lin, W., Li, J.H., Schüler, D., Jogler, C., Pan, Y.X., 2009. Diversity analysis of magnetotactic bacteria in Lake Miyun, northern China, by restriction fragment length polymorphism. Syst. Appl. Microbiol. 32, 342–350.

Lin, W., Pan, Y.X., 2009. Uncultivated Magnetotactic Cocci from Yuandadu Park in Beijing, China. Appl. Environ. Microbiol. 75, 4046–4052.

Lins, U., Keim, C.N., Evans, F.F., Farina, M., Buseck, P.R., 2007. Magnetite (Fe_3O_4) and greigite (Fe_3S_4) crystals in multicellular magnetotactic prokaryotes. Geomicrobiol. J. 24, 43–50.

Lins, U., McCartney, M.R., Farina, M., Frankel, R.B., Buseck, P.R., 2005. Habits of magnetosome crystals in coccoid magnetotactic bacteria. Appl. Environ. Microbiol. 71, 4902–4905.

Mann, S., Frankel, R.B., Blakemore, R.P., 1984a. Structure, morphology and crystal growth of bacterial magnetite. Nature 310, 405–407.

Mann, S., Moench, T.T., Williams, R.J.P., 1984b. A high resolution electron microscopic investigation of bacterial magnetite. Implications for crystal growth. Proc. R. Soc. B 221, 385–393.

Mann, S., Sparks, N.H.C., Blakemore, R.P., 1987a. Structure, morphology and crystal growth of anisotropic magnetite crystals in magnetotactic bacteria. Proc. R. Soc. Lond. B 231, 477–487.

Mann, S., Sparks, N.H.C., Blakemore, R.P., 1987b. Ultrastructure and characterization of anisotropic magnetic inclusions in magnetotactic bacteria. Proc. R. Soc. Lond. B 231, 469–476.

Matsunaga, T., Suzuki, T., Tanaka, M., Arakaki, A., 2007. Molecular analysis of magnetotactic bacteria and development of functional bacterial magnetic particles for nano-biotechnology. Trends Biotechnol. 25, 182–188.

McKay, D.S., Gibson, E.K., ThomasKeprta, K.L., Vali, H., Romanek, C.S., Clemett, S.J., Chillier, X.D.F., Maechling, C.R., Zare, R.N., 1996. Search for past life on Mars: Possible relic biogenic activity in Martian meteorite ALH84001. Science 273, 924–930.

Meldrum, F.C., Mann, S., Heywood, B.R., Frankel, R.B., Bazylinski, D.A., 1993a. Electron microscopy study of magnetosomes in a cultured Coccoid magnetotactic bacterium. P. Ror. Soc. Lond. B 251, 231–236.

Meldrum, F.C., Mann, S., Heywood, B.R., Frankel, R.B., Bazylinski, D.A., 1993b. Electron microscopy study of magnetosomes in two cultured Vibrioid magnetotactic bacteria. P. Ror. Soc. Lond. B 251, 237–242.

Moskowitz, B.M., Frankel, R.B., Bazylinski, D.A., 1993. Rock magnetic criteria for the detection of biogenic magnetite. Earth Planet. Sci. Lett. 120, 283–300.

Muxworthy, A.R., McClelland, E., 2000. Review of the low-temperature magnetic properties of magnetite from a rock magnetic perspective. Geophys. J. Int. 140, 101–114.

Muxworthy, A.R., Williams, W., 2009. Critical superparamagnetic/single-domain grain sizes in interacting magnetite particles: implications for magnetosome crystals. J. R. Soc. Interface 6, 1207–1212.

Pósfai, M., Kasama, T., Dunin-Borkowski, R.E., 2007. Characterization of bacterial magnetic nanostructures using high-resolution transmission electron microscopy and off-axis electron holography. In: Schüler, D. (Ed.), Magnetoreception and Magnetosomes in Bacteria. Springer-Verlag Berlin Heidelberg, Berlin, pp. 197–225.

Pósfai, M., Moskowitz, B.M., Arató, B., Schüler, D., Flies, C., Bazylinski, D.A., Frankel, R.B., 2006. Properties of intracellular magnetite crystals produced by *Desulfovibrio magneticus* strain RS-1. Earth Planet. Sci. Lett. 249, 444–455.

Pan, Y.X., Deng, C.L., Liu, Q.S., Petersen, N., Zhu, R.X., 2004. Biomineralization and magnetism of bacterial magnetosomes. Chin. Sci. Bull. 49, 2563–2568.

Pan, Y.X., Petersen, N., Davila, A.F., Zhang, L.M., Winklhofer, M., Liu, Q.S., Hanzlik, M., Zhu, R.X., 2005a. The detection of bacterial magnetite in recent sediments of Lake Chiemsee (southern Germany). Earth Planet. Sci. Lett. 232, 109–123.

Pan, Y.X., Petersen, N., Winklhofer, M., Davila, A.F., Liu, Q.S., Frederichs, T., Hanzlik, M., Zhu, R.X., 2005b. Rock magnetic properties of uncultured magnetotactic bacteria. Earth Planet. Sci. Lett. 237, 311–325.

Penninga, I., Dewaard, H., Moskowitz, B.M., Bazylinski, D.A., Frankel, R.B., 1995. Remanence measurements on individual magnetotactic bacteria using a pulsed magnetic-field. J. Magn. Magn. Mater. 149, 279–286.

Pradel, N., Santini, C.L., Bernadac, A., Fukumori, Y., Wu, L.F., 2006. Biogenesis of actin-like bacterial cytoskeletal filaments destined for positioning prokaryotic magnetic organelles. Prco. Natl. Acad. Sci. U. S. A. 103, 17485–17489.

Prozorov, R., Prozorov, T., Williams, T.J., Bazylinski, D.A., Mallapragada, S.K., Narasimhan, B., 2007. Magnetic irreversibility and Verwey transition in nano-crystalline bacterial magnetite. Phys. Rev. B 76. doi:10.1103/physRevB1176.054406.

Roberts, A.P., Pike, C.R., Verosub, K.L., 2000. First-order reversal curve diagrams: a new tool for characterizing the magnetic properties of natural samples. J. Geophys. Res. 105, 28461–28476.

Scheffel, A., Gruska, M., Faivre, D., Linaroudis, A., Plitzko, J.M., Schüler, D., 2006. An acidic protein aligns magnetosomes along a filamentous structure in magnetotactic bacteria. Nature 440, 110–114.

Schumann, D., Raub, T.D., Kopp, R.E., Guerquin-Kern, J.L., Wu, T.D., Rouiller, I., Smirnov, A.V., Sears, S.K., Lucken, U., Tikoo, S.M., Hesse, R., Kirschvink, J.L., Vali, H., 2008. Gigantism in unique biogenic magnetite at the Paleocene-Eocene Thermal Maximum. Proc. Natl. Acad. Sci. U. S. A. 105, 17648–17653.

Silva, K.T., Abreu, F., Keim, C.N., Farina, M., Lins, U., 2008. Ultrastructure and cytochemistry of lipid granules in the many-celled magnetotactic prokaryote, 'Candidatus Magnetoglobus multicellularis'. Micron 39, 1387–1392.

Simpson, E.T., Kasama, T., Pósfai, M., Buseck, P.R., Harrison, R.J., Dunin-Borkowski, R.E., 2005. Magnetic induction mapping of magnetite chains in magnetotactic bacteria at room temperature and close to the Verwey transition using electron holography. J. Phys.: Conf. Ser. 17, 108–121.

Sparks, N.H.C., Mann, S., Bazylinski, D.A., Lovley, D.R., Jannasch, H.W., Frankel, R.B., 1990. Structure and morphology of magnetite anaerobically-produced by a marine magnetotactic bacterium and a dissimilatory iron-reducing bacterium. Earth Planet. Sci. Lett. 98, 14–22.

Spring, S., Amann, R., Ludwig, W., Schleifer, K.H., van Gemerden, H., Petersen, N., 1993. Dominating role of an unusual magnetotactic bacterium in the microaerobic zone of a freshwater sediment. Appl. Environ. Microbiol. 59, 2397–2403.

Taylor, A.P., Barry, J.C., 2004. Magnetosomal matrix: ultrafine structure may template biomineralization of magnetosomes. J. Microsc. 213, 180–197.

Taylor, A.P., Barry, J.C., Webb, R.I., 2001. Structural and morphological anomalies in magnetosomes: possible biogenic origin for magnetite in ALH84001. J. Microsc. 201, 84–106.

Thomas-Keprta, K.L., Clemett, S.J., Bazylinski, D.A., Kirschvink, J.L., McKay, D.S., Wentworth, S.J., Vali, H., Gibson, E.K., Romanek, C.S., 2002. Magnetofossils from ancient Mars: a robust biosignature in the Martian meteorite ALH84001. Appl. Environ. Microbiol. 68, 3663–3672.

Thornhill, R.H., Burgess, J.G., Sakaguchi, T., Matsunaga, T., 1994. A morphological classification of bacteria containing bullet-shaped magnetic particles. FEMS Microbiol. Lett. 115, 169–176.

Vali, H., Forster, O., Amarantidis, G., Petersen, N., 1987. Magnetotactic bacteria and their magnetofossils in sediments. Earth Planet. Sci. Lett. 86, 389–400.

Vali, H., Kirschvink, J.L., 1990. Observations of magnetosome organization, surface structure, and iron biomineralization of undescribed magnetic bacteria: evolutionary speculations. In: Frankel, R.B., Blakemore, R.P. (Eds.), Iron Biominerals. Plenum Press, New York, pp. 97–115.